Electrochemical Reduction of Nitrate to Ammonia on Ultra-Stable Amorphous Co-P Electrocatalyst

Jin-Long Fan [1], Sheng-Bo Liu [3], Ming-Liang Chen [4], Zhang-Xiong Wu [1], Sheng-Peng Sun [1,*], and Yao-Yin Lou [1,2,*]

[1] School of Chemical and Environmental Engineering, College of Chemistry, Chemical Engineering and Materials Science, Soochow University, Suzhou, Jiangsu 215123, China

[2] CAS Key Laboratory of Urban Pollutant Conversion, Institute of Urban Environment, Chinese Academy of Sciences, Xiamen 361021, P. R. China

[3] Jiangsu Key Laboratory of Environmental Science and Engineering, School of Environmental Science and Engineering, Suzhou University of Science and Technology, Suzhou 215009, China

[4] Department of Chemical Engineering, Delft University of Technology, Van der Maasweg 9, Delft, 2629HZ, the Netherlands

* Corresponding authors: shepsun@suda.edu.cn; yylou@iue.ac.cn

Text S1:

Determination of ammonia-N:

A centrifuge tube was used to contain 125 μL of the electrolyte, followed by sequential addition of 125 μL of sulfuric acid at a concentration of 0.5 mol L^{-1}, 250 μL of buffer solution (pH = 7), 6 mL of ultra-pure water, and 250 μL of Nessler's reagent. After shaking, the mixture was allowed to stand for 30 minutes and then tested at 420 nm using an ultraviolet-visible spectrophotometer (Hach-DR3900).

Text S2:

Determination of nitrate-N and nitrite-N:

60 μL of the electrolyte was placed in a centrifuge tube, followed by the addition of 5.94 mL of ultra-pure water. The concentrations of nitrate-N and nitrite-N were then analyzed using an ion chromatograph (Thermo ICS-600) after shaking. For chromatography analysis, a mobile phase comprising of 4.5 mmol L^{-1} Na_2CO_3 and 0.8 mmol L^{-1} $NaHCO_3$ was utilized. The peak times for nitrite-N and nitrate-N at 11.2 min and 16.9 min, respectively.

Text S3:

***H radical quenching experiment:**

5,5-Dimethyl-1-pyrroline N-oxide (DMPO) was utilized to capture the unstable hydrogen radical. In brief, 5.0 mL of electrolyte was mixed with 20 μL of DMPO and deoxygenated by bubbling N_2. Potentiostatic electrolysis lasted for 5 minutes in the H-type cell under N_2 protection. ESR measurements were conducted on a JEX-320 spectrometer operated at a frequency close to 9.15 GHz, with a sweep frequency of 100 kHz and a power of 10 mW.

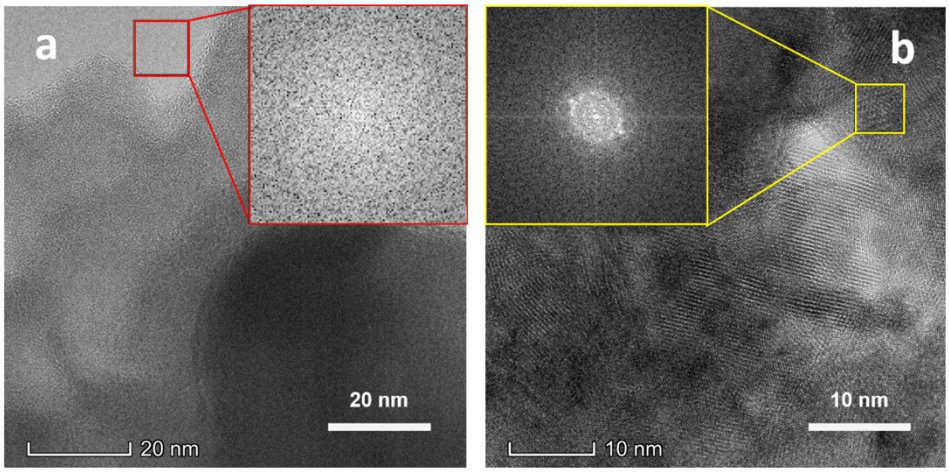

Figure S1. The TEM imagines of Co-P (a) and Co (b) catalysts. The insets are the corresponding electron diffraction of the two catalysts.

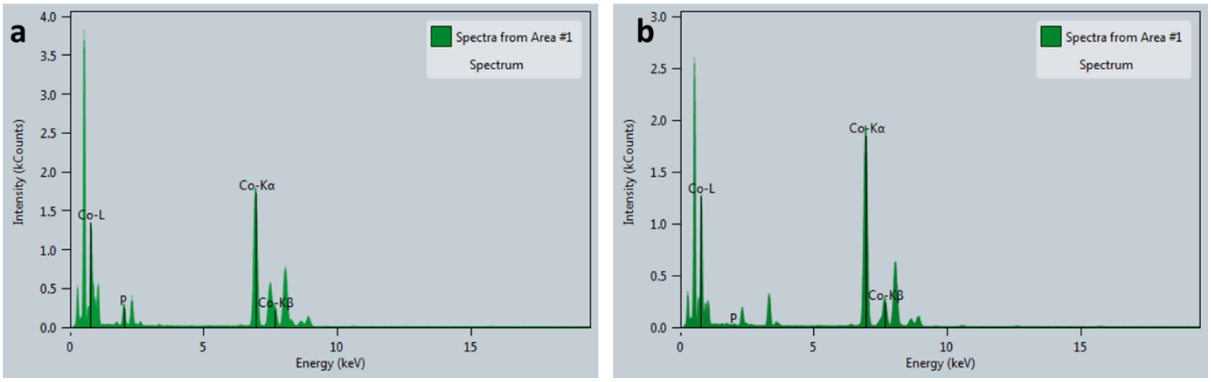

Figure S2. HRTEM-EDS analysis spectra of Co-P (a) and Co (b).

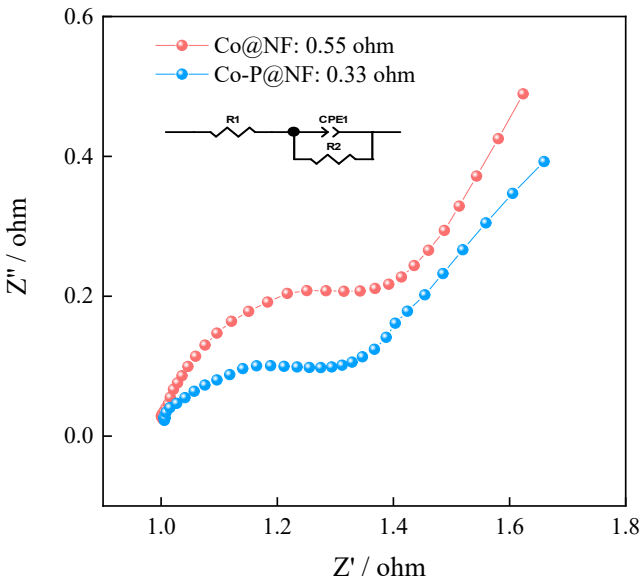

Figure S3. EIS analysis of Co and Co-P.

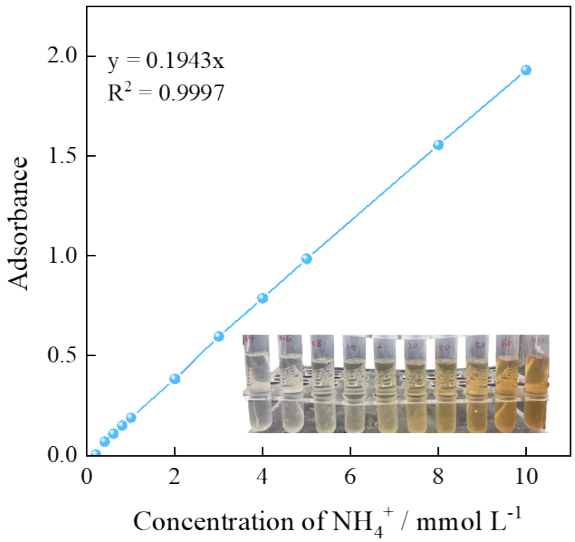

Figure S4. NH_3 calibration curves using Nessler Reagent method.

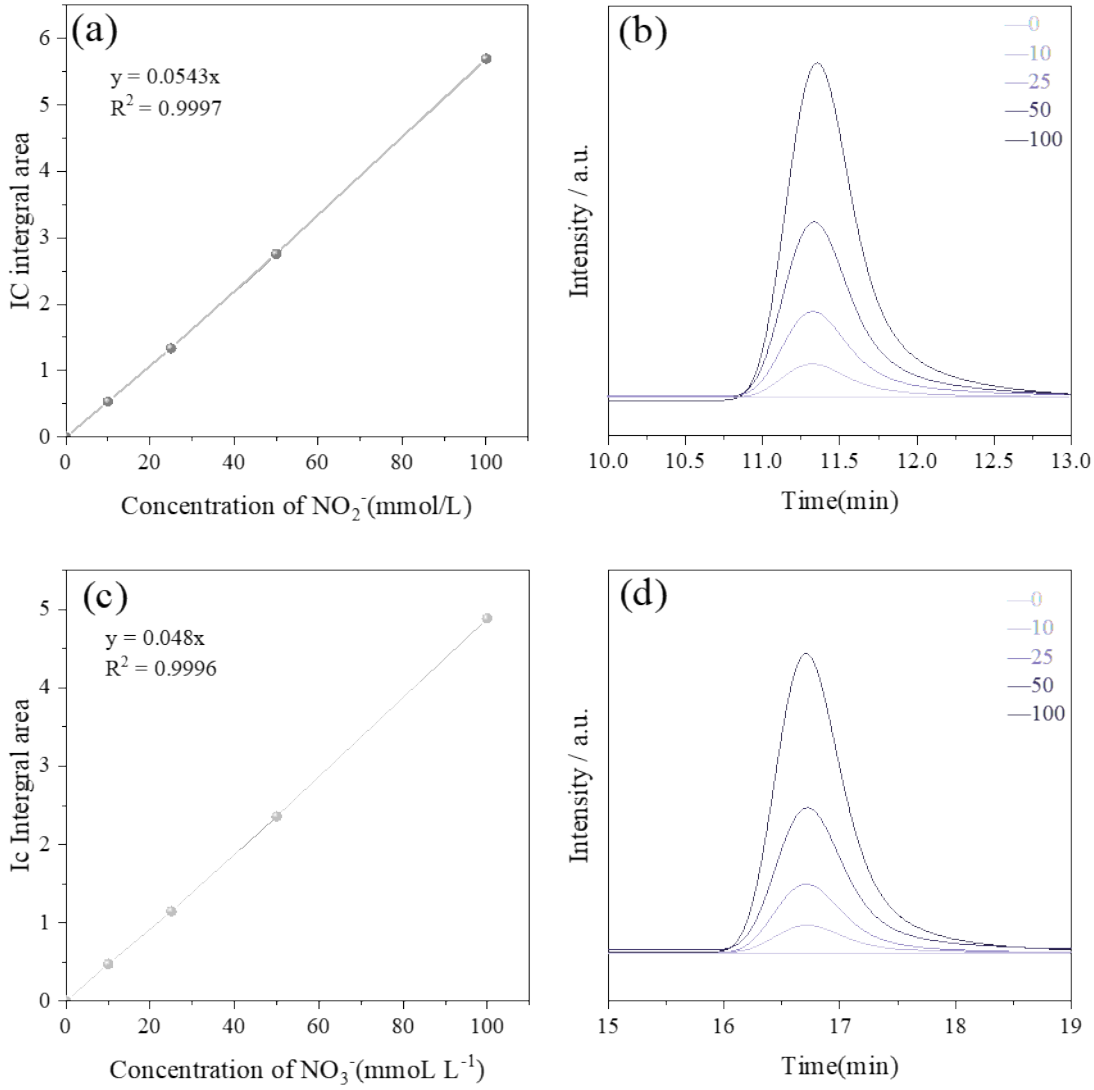

Figure S5. (a) Ionic chromatography calibration curves and (b) the corresponding chromatograms of NO_2^- in the concentration range of 0-100 mmol L^{-1} in which the solution environment is 0.1 mol L^{-1} KOH. (c) Ionic chromatography calibration curves and (d) the corresponding chromatograms of NO_3^- in the concentration range of 0-100 mmol L^{-1}.

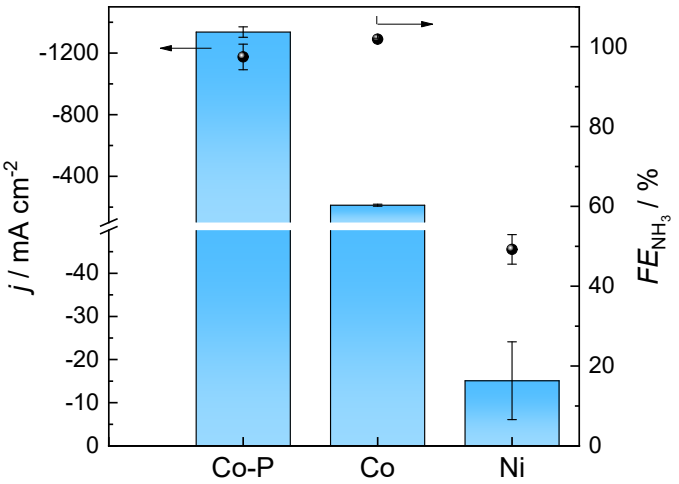

Figure S6. j and FE_{NH_3} over Co-P/NF, Co/NF, and Ni foam in 1 mol L^{-1} KOH with 0.1 mmol L^{-1} NO_3^- at -0.1 V vs. RHE.

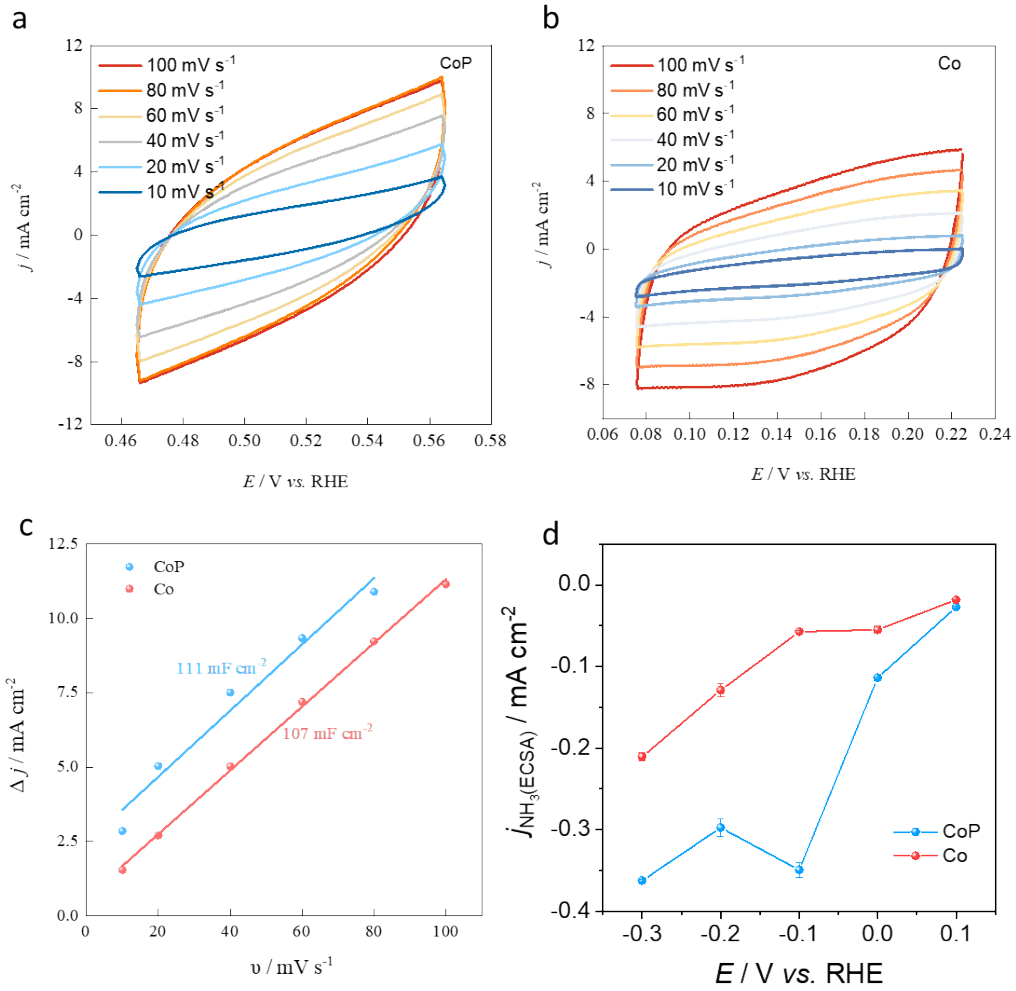

Figure S7. ECSA measurements of Co-P (a) and Co (b) and corresponding double layer capacitance (c). (Reference Cu foil: 29 μF cm^{-2}). (d) Bias-*j* for NH_3 normalized by ECSA for Co and CoP in 100 mM KNO_3 + 1M KOH

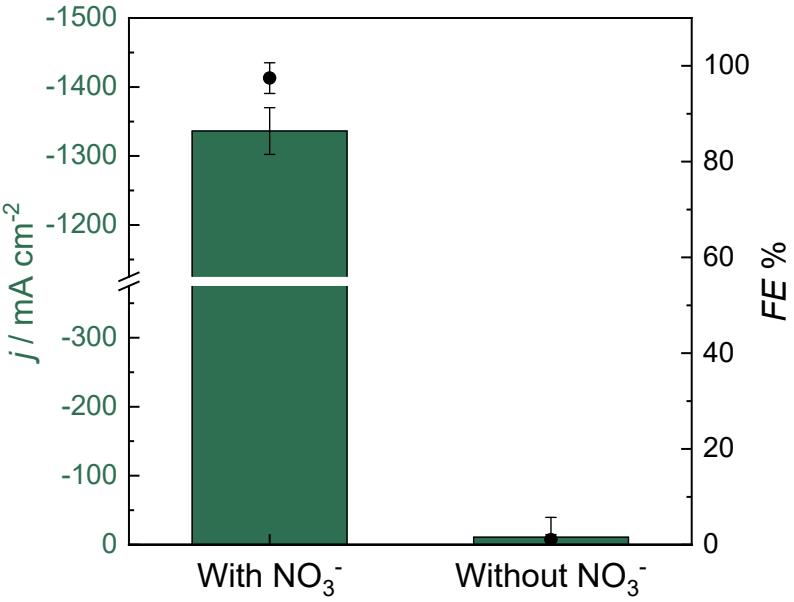

Figure S8. *j* and yield rate for NH_3 on Co-P@NF at -0.1 V *vs.* RHE in 1 M KOH electrolyte with or without 100 mM KNO_3.

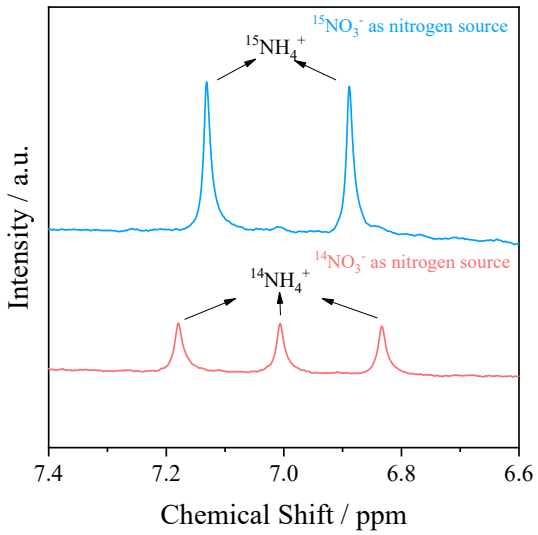

Figure S9. 1H NMR spectra of the electrolyte after $^{14}NO_3^-$ and $^{15}NO_3^-$ reduction at -0.1 V vs. RHE.

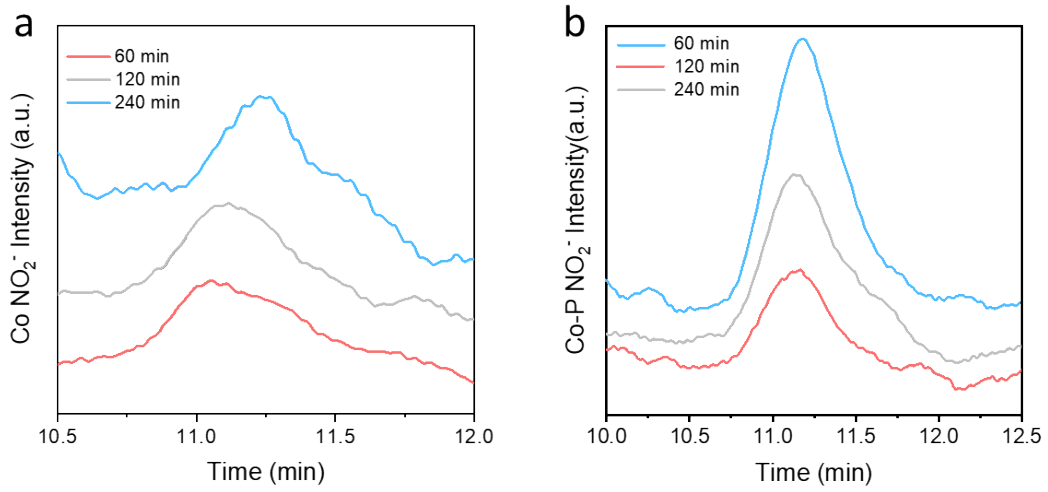

Figure S10. Ion chromatographic spectra of NO_2^- over Co (a) and Co-P (b) at open circle potential.

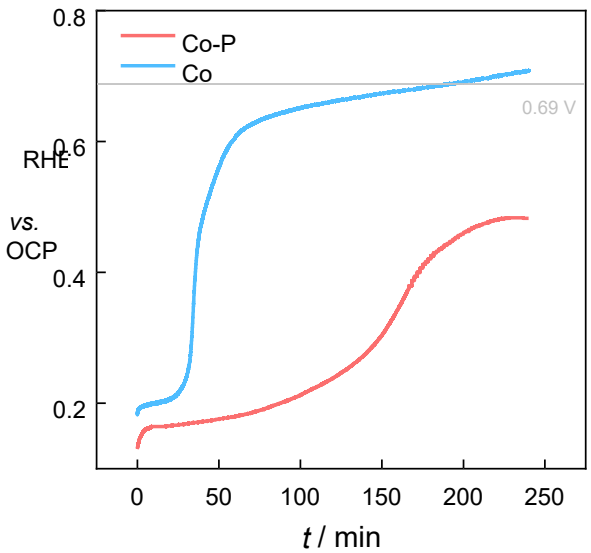

Figure S11. The open circle potential of Co and Co-P in 1 mol L^{-1} KOH with 0.1 mmol L^{-1} NO_3^-.

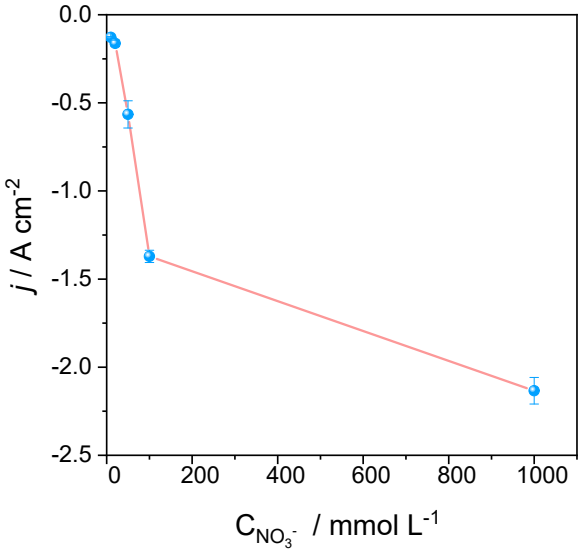

Figure S12. *j* over Co-P catalyst in the 1 mol L^{-1} KOH with different NO_3^- concentration.

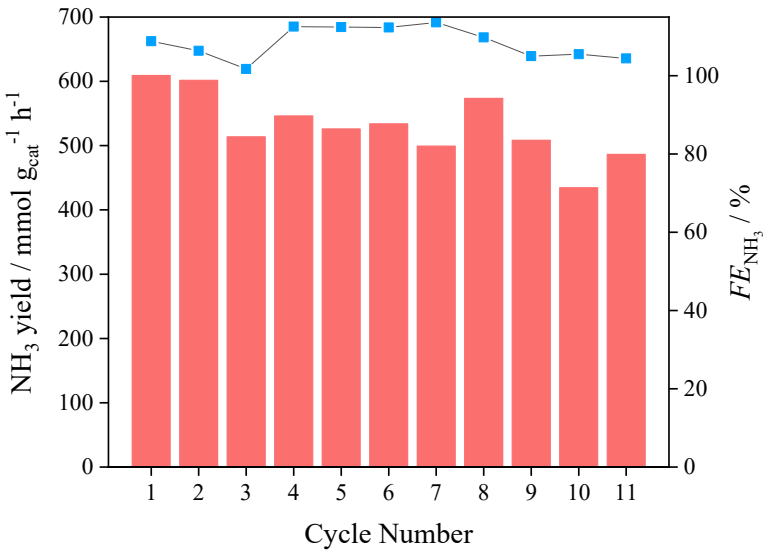

Figure S13. The cyclic stability of the catalysts towards NO_3^- reduction reaction.

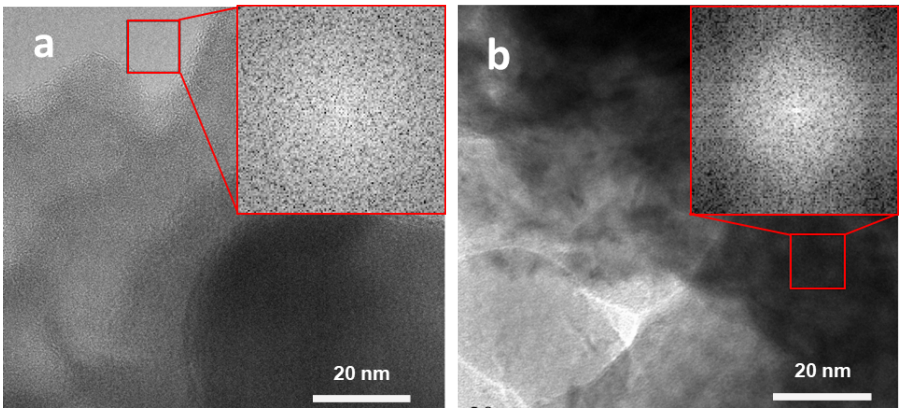

Figure S14. The TEM imagines of Co-P before (a) and after (b) long-term electrolysis. The insets are the corresponding electron diffractions of the chosen area.

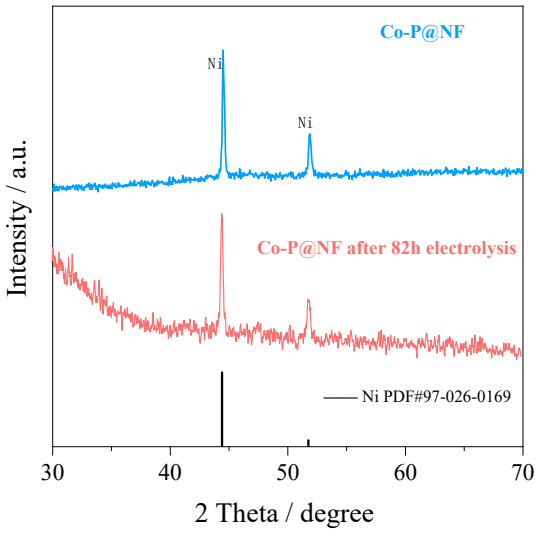

Figure S15. The XRD patterns of Co-P before (up) and after (bottom) long-term electrolysis.

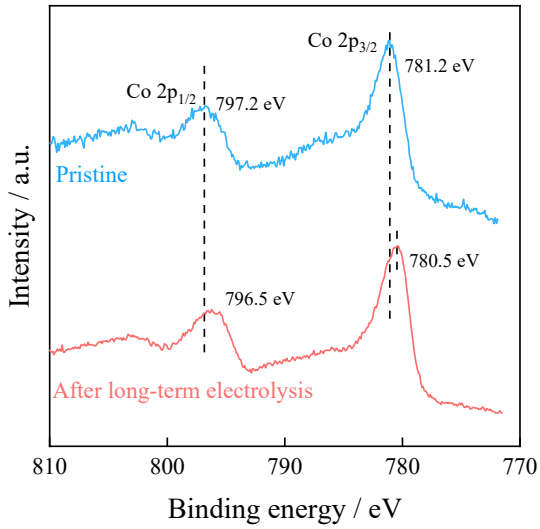

Figure S16. The XPS spectra of Co-P before (up) and after (bottom) long-term electrolysis.

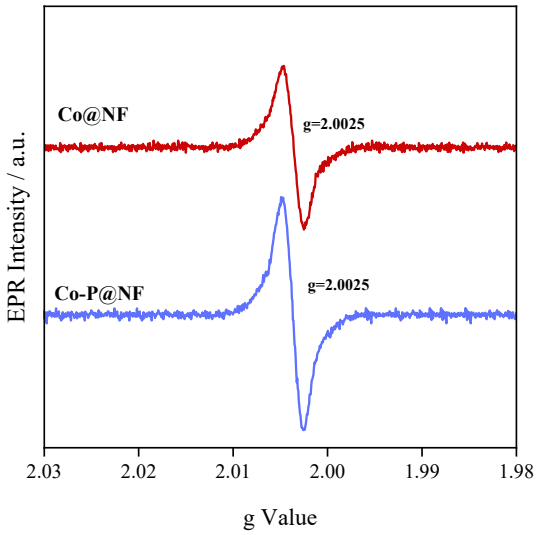

Figure S17. The electron paramagnetic resonance spectra of Co-P@NF and Co@NF.

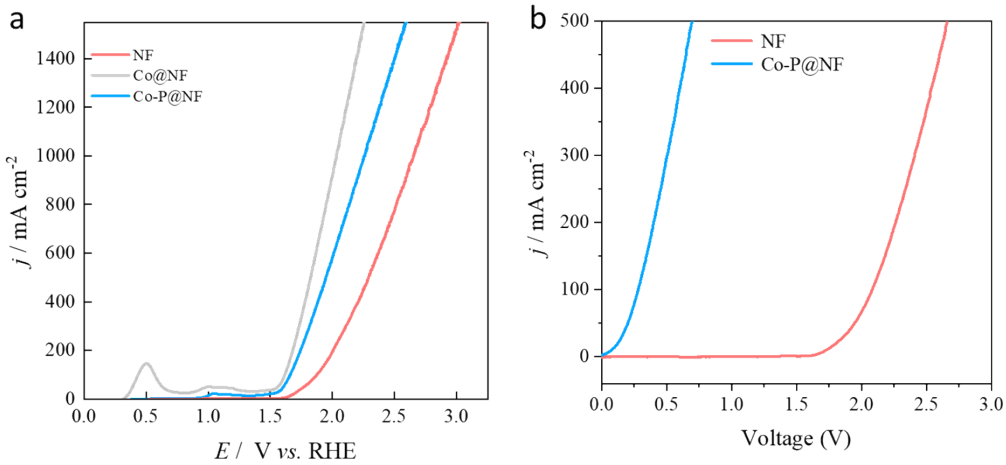

Figure S18. (a) Comparison LSV curves of NF between OER-NO_3^-RR and HzOR-NO_3^-RR. (b) LSV curves of obtained NF and Co-P@NF catalysts in HzOR-NO_3^-RR system

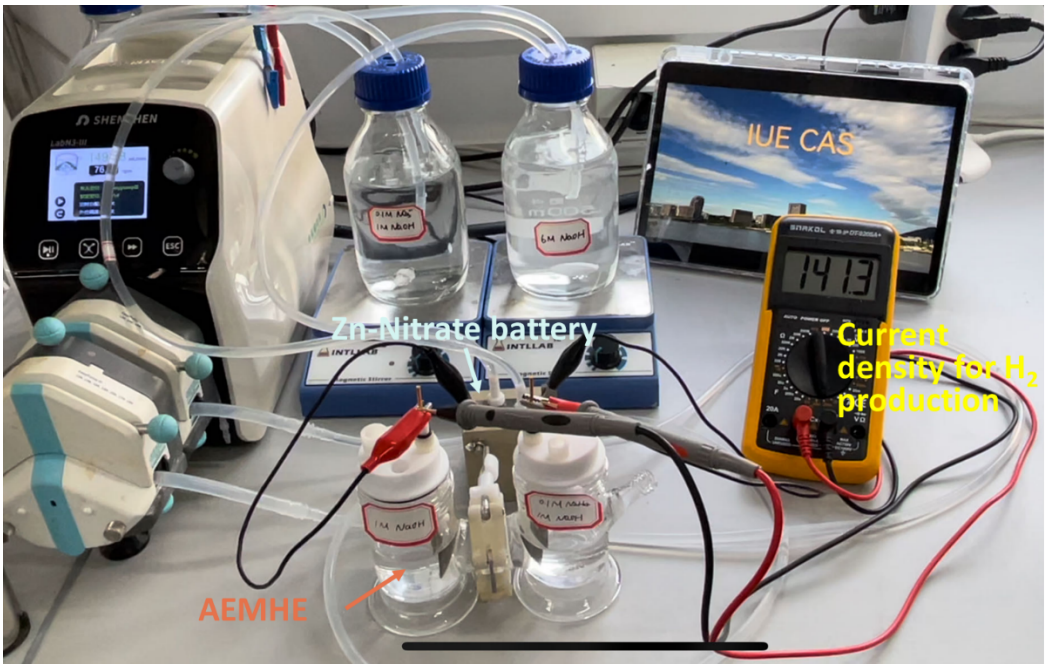

Figure S19. The current density of H_2 production in anion exchange membrane hydrazine electrolyzer (AEMHE), where the cathodic and anodic electrolytes are 1 M NaOH and 0.1 M NO_3^- + 1 M NaOH, and the cathode and anode are both Co-P@NF (2×2 cm^{-2}).

Table S1. HRTEM-EDS analysis spectra of Co and P in Co-P@NF

Element	Atomic fraction (%)	Atomic error (%)	Atomic fraction (%)	Atomic error (%)
	Co-P		Co	
P	13.05	1.5	0	--
Co	86.95	12.93	100	--

Table S2. Performance comparisons of Co-P@NF with previously reported electrocatalysts for NO_3^- to NH_3 electrocatalysis.

Cathode Material	electrolytes	Potential /V vs. RHE	FE/%	Current density / mA cm^{-2}	Refs
$Cu_{50}Ni_{50}$ alloy	1 M KOH, 0.1 M NO_3^-	-0.15	99	53	1
Cu-NBs-100	1 M KOH, 0.1 M NO_3^-	-0.15	95.3	288	2
HSCu-AGB@C	1 M KOH, 0.1 M NO_3^-	-0.2	94.2	239.4	3
Oxide derived Cu	1 M KOH, 0.1 M NO_3^-	− 0.15	92	137.5	4
Strained Ru nanoclusters	1 M KOH, 0.1 M NO_3^-	-0.2	100	120	5
FeB_2	1 M KOH, 0.1 M NO_3^-	-0.6	98.6	325	6
$CuCo_2O_4$/CFs	1 M KOH, 0.1 M NO_3^-	-0.3	81.9	40	7
CuCoSP on Cu foil	0.1 M KOH, 0.1 M NO_3^-	− 0.175	90.6	250.41	8
RuCo	1 M KOH, 0.1 M NO_3^-	0.071	98.4	250	9
V_{Co}-Co_3O_4/CC	0.1 M NaOH, 0.1 M NO_3^-	-0.4	97.2	75	10
Co-NAs	1 M KOH, 0.1 M NO_3^-	-0.1	97	500	11
CoO_x Nanosheets	0.1 M KOH, 0.1 M NO_3^-	-0.3	93.4	2.5	12
Co@NF	**1 M KOH, 0.1 M NO_3^-**	**-0.1**	**~100**	**212**	**This work**
Co-P@NF	**1 M KOH, 0.1**	**-0.1**	**97.5**	**1296**	**This work**

	M NO_3^-

References:

1 Wang, Y. *et al.* Enhanced Nitrate-to-Ammonia Activity on Copper–Nickel Alloys via Tuning of Intermediate Adsorption. *Journal of the American Chemical Society* **142**, 5702-5708, doi:10.1021/jacs.9b13347 (2020).

2 Hu, Q. *et al.* Reaction intermediate-mediated electrocatalyst synthesis favors specified facet and defect exposure for efficient nitrate–ammonia conversion. *Energy & Environmental Science* **14**, 4989-4997, doi:10.1039/d1ee01731d (2021).

3 Hu, Q. *et al.* Grain Boundaries Engineering of Hollow Copper Nanoparticles Enables Highly Efficient Ammonia Electrosynthesis from Nitrate. *CCS Chemistry* **4**, 2053-2064, doi:10.31635/ccschem.021.202101042 (2022).

4 Yuan, J., Xing, Z., Tang, Y. & Liu, C. Tuning the Oxidation State of Cu Electrodes for Selective Electrosynthesis of Ammonia from Nitrate. *ACS Applied Materials & Interfaces* **13**, 52469-52478, doi:10.1021/acsami.1c10946 (2021).

5 Li, J. *et al.* Efficient Ammonia Electrosynthesis from Nitrate on Strained Ruthenium Nanoclusters. *Journal of the American Chemical Society* **142**, 7036-7046, doi:10.1021/jacs.0c00418 (2020).

6 Zhang, G. *et al.* Tandem Electrocatalytic Nitrate Reduction to Ammonia on MBenes. *Angewandte Chemie International Edition* **62**, doi:10.1002/anie.202300054 (2023).

7 Niu, Z. *et al.* Bifunctional copper-cobalt spinel electrocatalysts for efficient tandem-like nitrate reduction to ammonia. *Chemical Engineering Journal* **450**, doi:10.1016/j.cej.2022.138343 (2022).

8 He, W. *et al.* Splicing the active phases of copper/cobalt-based catalysts achieves high-rate tandem electroreduction of nitrate to ammonia. *Nature Communications* **13**, doi:10.1038/s41467-022-28728-4 (2022).

9 Zhu, W. *et al.* Weakened d–p orbital hybridization inin situreconstructed Ru/β-Co(OH)2heterointerfaces for accelerated ammonia electrosynthesis from nitrates. *Energy & Environmental Science* **16**, 2483-2493, doi:10.1039/d3ee00371j (2023).

10 Deng, Z. *et al.* High-Efficiency Electrochemical Nitrate Reduction to Ammonia on a Co3O4 Nanoarray Catalyst with Cobalt Vacancies. *ACS Applied Materials & Interfaces* **14**, 46595-46602, doi:10.1021/acsami.2c12772 (2022).

11 Deng, X., Yang, Y., Wang, L., Fu, X. Z. & Luo, J. L. Metallic Co Nanoarray Catalyzes Selective NH3 Production from Electrochemical Nitrate Reduction at Current Densities Exceeding 2 A cm−2. *Advanced Science* **8**, doi:10.1002/advs.202004523 (2021).

12 Wang, J. *et al.* Electrocatalytic Reduction of Nitrate to Ammonia on Low-Cost Ultrathin CoOx Nanosheets. *ACS Catalysis* **11**, 15135-15140, doi:10.1021/acscatal.1c03918 (2021).